Giant nonlocal Kerr nonlinearity and polaritonic solitons in a Rydberg-dressed Bose-Einstein condensate

YUXI CHEN,[1] ZHENGYANG BAI,[1] CHAO HANG,[1,2,3,*] AND GUOXIANG HUANG[1,2,3]

[1]*State Key Laboratory of Precision Spectroscopy, East China Normal University, Shanghai 200241, China*
[2]*NYU-ECNU Institute of Physics, New York University at Shanghai, Shanghai 200062, China*
[3]*Collaborative Innovation Center of Extreme Optics, Shanxi University, Taiyuan, Shanxi 030006, China*
[*]*chang@phy.ecnu.edu.cn*

Abstract: We present a scheme to generate nonlocal optical Kerr nonlinearity and polaritonic solitons via matter-wave superradiance in a Rydberg-dressed Bose-Einstein condensate (BEC). We show that the polariton spectrum of the scattered field generated by the superradiance is changed significantly due to the existence of the long-range Rydberg-Rydberg interaction between atoms, i.e. it has a roton-maxon form; moreover, the BEC structure factor displays a strong dependence on the Rydberg-dressing, which can be tuned in a controllable way. We also show that such a Rydberg-dressed BEC system can support a giant nonlocal optical Kerr nonlinearity, and hence allow the formation and stable propagation of polaritonic solitons, which have ultraslow propagation velocity and ultralow generation power. The results reported here are useful to understand the unique properties of Rydberg-dressing in BECs and have potential applications in optical information processing and transmission.

1. Introduction

Realization of strong nonlinear interactions between dilute atomic ensembles and weak optical fields have attracted growing attentions in recent years due to diverse applications in quantum computation and quantum information, high-precision sensing, simulation of many-body physics, and so on [1,2]. Particularly, light propagation through near-resonance atomic gases with the use of coherent multi-photon process (such as Raman process and electromagnetically induced transparency) has been proved to be a very promising approach for realizing the strong nonlinear interactions between photons [3–11]. In addition, under the excitation of a laser field, collective atomic recoil motion, also known as matter-wave superradiance, may occur [12–14]. The collective center-of-mass recoil motion of ultracold atoms is an intriguing process, where a group of atoms in the same electronic state can recoil coherently; the recoiled atoms can mediate the conversion of atomic kinetic energy into radiation, resulting in the generation of scattered laser fields.

In early experiments on the matter-wave superradiance [15–17], an elongated Bose-Einstein condensate (BEC) was used, and a long-duration pump laser field was sent along the short transverse direction of the BEC. In such a scheme, the scattered laser field is dominated by the axial or end-fire modes, while the recoiled atoms from the BEC form special fan-like or X-shaped scattering patterns in the momentum space (alias as the side-mode distribution) depending on the duration and strength of the incident laser pulse. Since then, comprehensive studies for understanding the underlying physics of these experimental observations were carried out, providing further insights into the features of the atomic momentum distribution [18–24] and the coupled dynamics of matter waves and laser fields [25,26]. Meanwhile, superradiant scattering and polariton formation from an elongated BEC with the incident laser along the long axis was

also investigated, where the asymmetric backward scattering pattern and multi-matter-optical wave-mixing process were found [27–31]. Recent experimental and theoretical works also revealed that matter-wave superradiance can be achieved in degenerate fermion gases [30]. In addition to its fundamental role for atom optics [32] and related research fields, the study of matter-wave superradiance opens possibilities for many practical applications such as matter-wave amplifiers, highly sensitive matter-wave interferometers, quantum information processors based on ultracold atoms, and so on. Up to now, however, the collective atomic recoil motion has been demonstrated for ultracold atoms with only short-range contact interactions.

On the other hand, much attention has been paid to the study of ultracold Rydberg atomic gases [33,34] in recent years, which exhibit strong and long-range interactions. Due to the large electric-dipole moment of Rydberg states, the interaction between two Rydberg atoms can reach several megahertz at their separation of several micrometers [35,36], which may generate giant nonlocal optical Kerr nonlinearity when such atoms are coupled with laser fields [37–44]. However, lifetimes of Rydberg states are typically 10-100 μs, which are much shorter than BEC lifetimes and are not long enough to explore a wave propagation phenomenon. In order to overcome this drawback, Rydberg dressing, in which a far-detuned laser field couples electronic ground states to Rydberg states, is proposed [45–49]. The Rydberg dressing renders a long-range, soft-core type interaction between Rydberg-dressed atoms, whose coherence time and interaction strength can be controlled by the coupling laser. Particularly, the coherence time of Rydberg-dressed atoms can be prolonged to 10-100 ms, which is comparable with BEC lifetimes. Recent experiments have successfully demonstrated Rydberg-dressing in optical tweezers [50], optical lattices [51–53], and traps [54–56]; many interesting physics associated with Rydberg-dressing such as magnets [52], transport [57], wave mixing [58], supersolids [46,59–61], and experimental observation [62] have also been studied. Different from BECs with dipolar interactions, the Rydberg-dressing in the BECs without dipolar interaction gives rise to isotropic interaction potentials, which is crucial for the stabilization of BECs [45,46].

In this article, we present a scheme to create giant nonlocal optical Kerr nonlinearity and ultraslow polaritonic solitons via matter-wave superradiance in a Rydberg-dressed BEC. The system under consideration is a cigar-shaped BEC, which interacts with a pump and a control laser fields, propagating along the long-axis direction of the BEC. The pump field couples the ground state and an excited state, while the control field couples the excited state and a high-lying Rydberg state. Due to such a coupling configuration, the BEC acquires a collective atomic recoil motion from the pump and control lasers and a scattered laser field is spontaneously generated and propagates along the same direction with the pump field (i.e. along the long-axis direction of the BEC).

We show that, due to the existence of the long-range Rydberg-Rydberg interaction between the atoms, the polariton spectrum (linear dispersion relation) of the scattered laser field generated by the superradiance is changed significantly comparing with the case without the Rydberg-Rydberg interaction. Particularly, when the strength of the Rydberg-Rydberg interaction increases, the spectrum can develop a maxon maximum followed by a roton minimum, which ultimately results in a roton instability. Furthermore, we find that the BEC structure factor has a strong dependence on the property of the Rydberg-dressing, which is much easier to be manipulated than that in conventional BECs with only short-range interactions.

We demonstrate that by using such a system a giant nonlocal optical Kerr nonlinearity can be achieved, which is also contributed by the strong and long-range Rydberg-Rydberg interaction. Based on such result, the formation and robust propagation of polaritonic solitons (i.e. collective nonlinear excitations of the Rydberg-dressed BEC coupled with the scattered laser field) through a backward scattering process can be realized. Moreover, such solitons have ultraslow propagation velocity and can be generated with ultralow light power. The results reported here are useful for

the understanding of the unique properties of Rydberg-dressing in ultracold atomic gases (BECs) and have potential applications in optical information processing and transmission.

The remainder of the paper is organized as follows. In Sec. 2, we describe the physical model under study. In Sec. 3, we make the asymptotic expansion on the model equations and calculate the polariton spectrum and the structure factor of Rydberg-dressed BEC. In Sec. 4, we derive the nonlinear envelope equation controlling the evolution of nonlinear polaritons and investigate the nonlocal Kerr nonlinearity and polaritonic solitons. The last section contains the summary of the main results of the present work.

2. Physical model

We consider a ultracold three-state atomic gas with a ladder-shaped level configuration where the atoms are initially populated in the ground state $|1\rangle$. We assume that the atoms are trapped in a highly anisotropic trapping potential $V(\mathbf{r})$, and they form a cigar-shaped BEC, with its long axis along z direction; see Fig. 1(a). We also assume that a pump laser field $\mathbf{E}_P$ (with the angular frequency ω_P and the wavevector $\mathbf{k}_P$) and a control laser field $\mathbf{E}_C$ (with the angular frequency ω_C and the wavevector $\mathbf{k}_C$) are applied to the BEC and they are all linearly polarized along the x axis and propagate along the z direction. The pump laser field couples the transition from the ground state to an excited state $|2\rangle$, while the control laser field couples the transition from the excited state to a high-lying Rydberg state $|3\rangle$; see Fig. 1(c).

To make the system work in a Rydberg-dressed regime, we further assume that the control field is sufficiently detuned from the related one-photon resonance, so that the excitation of the atoms in the Rydberg state $|3\rangle$ can be significantly suppressed. In such a regime, the excited state is dressed by the Rydberg state through the far-off-resonant coupling of the control field; the atomic gas can be described by a reduced two-state system (see the Supplement 1).

Due to the gain provided by the pump laser field, a weak scattered laser field (with the center angular frequency ω_S and the center wavenumber $\mathbf{k}_S$) will emerge, which radiates from the excited state $|2\rangle$ to the ground state $|1\rangle$. Thereby, the total electric-field vector in the system can be written as $\mathbf{E} = \sum_{\alpha=P,C,S} \mathbf{E}_\alpha = \sum_{\alpha=P,C,S} \mathbf{e}_\alpha \mathcal{E}_\alpha e^{i(\mathbf{k}_\alpha \cdot \mathbf{r} - \omega_\alpha t)} +$ c.c., where $\mathbf{e}_P$, $\mathbf{e}_C$ and $\mathbf{e}_S$ ($\mathcal{E}_P$, $\mathcal{E}_C$ and $\mathcal{E}_S$) are respectively polarization unit vectors and amplitudes of the pump, control and scattered fields; c.c. denotes the corresponding complex conjugate terms. Because of the cigar-shaped geometry of the BEC, the scattered field has nearly the same polarization direction with the pump and control fields, i.e. $\mathbf{e}_S = \mathbf{e}_P = \mathbf{e}_C = \mathbf{e}_x$, and propagates along the long-axis of the BEC, i.e. $\mathbf{k}_S \cdot \mathbf{r} \approx k_S z$. Generally, the spontaneously generated scattered field propagates co-linearly and anti-co-linearly with the pump field, as illustrated in Fig. 1(a) and Fig. 1(b), respectively. The wavevector of the recoiled atoms is then determined by $\Delta \mathbf{k} = \mathbf{k}_P - \mathbf{k}_S$ for the forward scattering and $\Delta \mathbf{k} = \mathbf{k}_P + \mathbf{k}_S$ for the backward scattering.

The dynamics of the BEC and the laser fields can be described by the Hamiltonian $\hat{H} = \hat{H}_{\text{atom}} + \hat{H}_{\text{laser}} + \hat{H}_{\text{int}}$, where

$$\hat{H}_{\text{atom}} = \sum_{\alpha=1}^{3} \int d^3r \left\{ \hbar\omega_\alpha \hat{\Psi}_\alpha^\dagger(\mathbf{r},t)\hat{\Psi}_\alpha(\mathbf{r},t) + \hat{\Psi}_\alpha^\dagger(\mathbf{r},t)H_0\hat{\Psi}_\alpha(\mathbf{r},t) \right\}$$

$$+ \sum_{\alpha,\beta=1}^{3} \frac{1}{2} \int \int d^3r d^3r' \hat{\Psi}_\alpha^\dagger(\mathbf{r},t)\hat{\Psi}_\beta^\dagger(\mathbf{r}',t)U_{\alpha\beta}(\mathbf{r}-\mathbf{r}')\hat{\Psi}_\beta(\mathbf{r}',t)\hat{\Psi}_\alpha(\mathbf{r},t),$$

(1a)

$$\hat{H}_{\text{laser}} = \frac{1}{2} \int d^3r \epsilon_0 \mathbf{E}(\mathbf{r},t)^2,$$

(1b)

$$\hat{H}_{\text{int}} = - \sum_{\alpha,\beta=1}^{3} \int d^3r \hat{\Psi}_\alpha^\dagger(\mathbf{r},t)[\mathbf{p}_{\alpha\beta} \cdot \mathbf{E}(\mathbf{r},t)]\hat{\Psi}_\beta(\mathbf{r},t),$$

(1c)
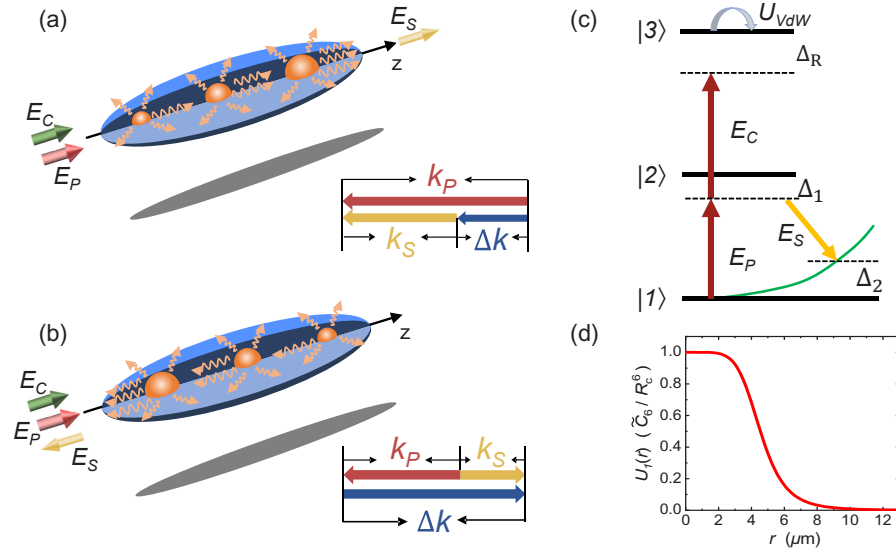
Fig. 1. Excitation scheme, level diagram, and nonlocal response function of the cigar-shaped Rydberg-dressed BEC, which interacts with a pump laser field $\mathbf{E}_P$ (wavevector $\mathbf{k}_P$) and a control laser field $\mathbf{E}_C$ (wavevector $\mathbf{k}_C$), propagating along the long-axis (z) direction of the BEC. A scattered laser field $\mathbf{E}_S$ (wavevector $\mathbf{k}_S$) can spontaneously emerge in the system, propagating co-linearly or anti-co-linearly with the pump field. (a) Excitation scheme for the forward scattering. Inset: relation between $\mathbf{k}_P$ and $\mathbf{k}_S$, with $\Delta\mathbf{k} = \mathbf{k}_P - \mathbf{k}_S$. (b) The same as (a) but for the excitation scheme of backward scattering, with $\Delta\mathbf{k} = \mathbf{k}_P + \mathbf{k}_S$. (c) Ladder-type energy-level diagram of the atoms, in which the pump field $\mathbf{E}_P$ couples the ground state $|1\rangle$ to the excited state $|2\rangle$ (with detuning Δ_1) and the control field $\mathbf{E}_C$ far-off-resonantly couples $|2\rangle$ to the Rydberg state $|3\rangle$ (with detuning Δ_R). A weak scattered field $\mathbf{E}_S$ radiates from the excited state $|2\rangle$ to the ground state $|1\rangle$ (with detuning Δ_2). The interaction between Rydberg atoms is described by the van der Waals potential $U_{\text{VdW}} = \hbar C_6/|\mathbf{r} - \mathbf{r}'|^6$ (C_6 is the dispersion parameter). (d) Long-range soft-core interaction potential $U_1(r)$, scaled by $\tilde{C}_6/R_c^6$ ($\tilde{C}_6$ is the modified dispersion parameter; R_c is the Rydberg blockade radius), as a function of the separation $r = |\mathbf{r} - \mathbf{r}'|$ between two Rydberg atoms (locate at $\mathbf{r}$ and $\mathbf{r}'$, respectively) for the principle quantum number $n = 60$.

with $H_0 = -[\hbar^2/(2M)]\nabla^2 + V(\mathbf{r})$, $d^3r = dxdydz$, and $d^3r' = dx'dy'dz'$. Here $\hat{\Psi}_\alpha$ is the atomic field operator related to the state $|\alpha\rangle$ ($\alpha = 1, 2, 3$), obeying the commutation relations $[\hat{\Psi}_\alpha(\mathbf{r},t), \hat{\Psi}_\beta(\mathbf{r}',t)] = [\hat{\Psi}_\alpha^\dagger(\mathbf{r},t), \hat{\Psi}_\beta^\dagger(\mathbf{r}',t)] = 0$ and $[\hat{\Psi}_\alpha(\mathbf{r},t), \hat{\Psi}_\beta^\dagger(\mathbf{r}',t)] = \delta_{\alpha\beta}\delta(\mathbf{r} - \mathbf{r}')$, M is the atomic mass, $V(\mathbf{r})$ is a harmonic trapping potential which is assumed to be the same for the three atomic internal states, and $\mathbf{p}_{\alpha\beta}$ is the electric dipole matrix element for the transition between the states $|\alpha\rangle$ and $|\beta\rangle$, with $\mathbf{p}_{\alpha\alpha} = 0$ and $\mathbf{p}_{\alpha\beta} = \mathbf{p}_{\beta\alpha}^*$.

From the Hamiltonian, one can obtain the Heisenberg equations for $\hat{\Psi}_\alpha$, i.e. $i\hbar\partial\hat{\Psi}_\alpha/\partial t = [\hat{\Psi}_\alpha, \hat{H}]$ ($\alpha = 1, 2, 3$). We emphasize that the present system is studied under the following conditions: (i) The BEC is initially prepared in the ground state $|1\rangle$; (ii) The two-photon detuning Δ_R is enough large (order of GHz) so that the atomic excitation of the Rydberg state $|3\rangle$ is not significant and the system works in a Rydberg-dressed regime; (iii) The one-photon detuning Δ_1 is also large (order of tens of MHz), and hence the spontaneous emission from the excited state $|2\rangle$ can be largely suppressed and the system works in a dispersive nonlinearity regime; (iv) The interatomic interactions are described by the two-body potential with the form $U_{\alpha\beta}(\mathbf{r} - \mathbf{r}') = \delta_{\alpha 1}\delta_{\beta 1}U_0\delta(\mathbf{r} - \mathbf{r}') + \delta_{\alpha 3}\delta_{\beta 3}U_{\text{vdW}}(\mathbf{r} - \mathbf{r}')$. Here, the first (second) term on the right hand side describes the contact [van der Waals (vdW)] interaction between the atoms in

the ground state $|1\rangle$ (Rydberg state $|3\rangle$) located at $\mathbf{r}$ and $\mathbf{r}'$, respectively [45,46]. The parameter $U_0 = 4\pi\hbar^2 a_s/M$, with a_s the s-wave scattering length; the vdW interaction potential has the form of $U_{\mathrm{vdW}}(\mathbf{r}, \mathbf{r}') = \hbar C_6/|\mathbf{r} - \mathbf{r}'|^6$, with C_6 the dispersion parameter ($C_6 \propto n^{11}$; n is the principle quantum number of the Rydberg state) [34–36].

Under the above assumptions, we adiabatically eliminate the equations for the motion of $\hat{\Psi}_2$ and $\hat{\Psi}_3$. Then, by employing mean-field approximation to $\hat{\Psi}_1$, i.e. $\hat{\Psi}_1 \rightarrow \langle\hat{\Psi}_1\rangle \equiv \Psi$, we can obtain the Gross-Pitaevskii (GP) equation for the condensate wave function Ψ, reading

$$i\hbar\frac{\partial}{\partial t}\Psi = -\frac{\hbar^2}{2M}\nabla^2\Psi + V(\mathbf{r})\Psi + \int d^3r' U(\mathbf{r} - \mathbf{r}')|\Psi(\mathbf{r}')|^2\Psi(\mathbf{r})$$
$$-\frac{|\mathbf{p}_{12} \cdot \mathbf{E}^{(+)}(\mathbf{r}, t)|^2}{\hbar\Delta_1}\Psi - i\hbar\Gamma(\mathbf{r}, t)\Psi, \tag{2}$$

where $\nabla = (\partial_x, \partial_y, \partial_z)$, $\mathbf{E}^{(+)} = \mathbf{e}_x[\mathcal{E}_P e^{i(k_P z - \omega_P t)} + \mathcal{E}_S(x, y, z, t)e^{i(k_S z - \omega_S t)}]$, $U(\mathbf{r} - \mathbf{r}') = U_0\delta(\mathbf{r}) + U_1(\mathbf{r} - \mathbf{r}')$ (with $U_1(\mathbf{r} - \mathbf{r}') \equiv \hbar\tilde{C}_6/(|\mathbf{r} - \mathbf{r}'|^6 + R_c^6)$ an effective soft-core-shaped two-body interaction potential), and $\Gamma(\mathbf{r}, t) = |\mathbf{p}_{12} \cdot \mathbf{E}^{(+)}(\mathbf{r}, t)|^2\Gamma_{12}/(\hbar^2\Delta_1^2)$ is effective decay rate (with Γ_{12} the spontaneous decay rate from $|2\rangle$ to $|1\rangle$). Here $\tilde{C}_6$ is the modified dispersion parameter and R_c is the Rydberg blockade radius [45,46], both of which are proportional to C_6. Figure 1(d) shows the soft-core-shaped interaction potential U_1 as a function of $r = |\mathbf{r} - \mathbf{r}'|$ for $n = 60$ (scaled by $\tilde{C}_6/R_c^6$).

The equation of motion for the electric field can be obtained from the Maxwell equation $\partial^2\mathbf{E}^{(+)}/\partial t^2 = c^2\nabla^2\mathbf{E}^{(+)} - (1/\epsilon_0)\partial^2\mathbf{P}^{(+)}/\partial t^2$, where $\mathbf{P}^{(+)} = \mathbf{p}_{12}(\mathbf{p}_{21} \cdot \mathbf{E}^{(+)})|\Psi|^2/(\hbar\Delta_1)$ is the electric polarization vector related to $\mathbf{E}^{(+)}$ [25–27]. Under the slowly varying envelope approximation, the Maxwell equation is reduced to

$$i\left(\frac{\partial}{\partial z} + \frac{1}{c}\frac{\partial}{\partial t}\right)\mathcal{E}_S + \frac{c}{2\omega_S}\nabla_\perp^2\mathcal{E}_S + \frac{c}{2\omega_S}\left(k_P^2 - \frac{\omega_P^2}{c^2}\right)\mathcal{E}_P e^{i[\Delta k z - \Delta_2 t]}$$
$$= \frac{\omega_S}{2\epsilon_0 c}\frac{|\mathbf{p}_{12} \cdot \mathbf{e}_x|^2}{\hbar\Delta_1}|\Psi|^2(\mathcal{E}_S + \mathcal{E}_P e^{i[\Delta k z - \Delta_2 t]}), \tag{3}$$

where $\nabla_\perp = (\partial_x, \partial_y)$, $\Delta k = k_P - k_S$ ($\Delta k = k_P + k_S$) corresponds to the forward (backward) scattering and $\Delta_2 = \omega_P - \omega_S$. If there is no atoms, $|\Psi|^2 = 0$, the scattered field will vanish ($\Omega_S = 0$) and one can get $k_P = \omega_P/c$, which is the dispersion relation for the pump field in the absence of atoms.

The GP Eq. (2) and Maxwell Eq. (3) are both (3+1)D. To simplify the problem, we assume that the Rydberg-dressed BEC is trapped in a highly anisotropic potential of the form $V(\mathbf{r}) = (M/2)[\omega_\perp^2(x^2 + y^2) + \omega_z^2 z^2]$, with $\omega_\perp \gg \omega_z$. Thus, the BEC is elongated along the z axis but remains symmetric in the transverse (x and y) directions. By introducing the dimensionless variables $(\xi, \eta) = a_\perp^{-1}(x, y)$ (with $a_\perp = \sqrt{\hbar/(M\omega_\perp)}$ the harmonic oscillator length in the transverse directions), $\zeta = a_z^{-1}z$ (with $a_z = \sqrt{\hbar/(M\omega_z)}$ the harmonic oscillator length in the longitudinal direction), $\tau = \omega_\perp t$, $\psi = \Psi/\sqrt{N_0}$ (with $N_0 = N/a_\perp^3$ the atomic density), and $\varepsilon_S = \mathcal{E}_S/\mathcal{E}_P$, Eq. (2) can be written into a dimensionless form

$$i\frac{\partial\psi}{\partial\tau} = -\frac{1}{2}\tilde{\nabla}^2\psi + \frac{1}{2}(\xi^2 + \eta^2)\psi + \frac{1}{2}\frac{\omega_z^2}{\omega_\perp^2}\zeta^2\psi + \frac{4\pi Na_s}{a_\perp}|\psi|^2\psi$$
$$+ \frac{N}{\hbar\omega_\perp}\iiint d\xi' d\eta' d\zeta' U_1(\xi' - \xi, \eta' - \eta, \zeta' - \zeta)|\psi(\xi', \eta', \zeta')|^2\psi(\xi, \eta, \zeta) \tag{4}$$
$$- \frac{|\Omega_P|^2}{\omega_\perp\Delta_1}(1 + \varepsilon_S e^{-i\Phi} + \varepsilon_S^* e^{i\Phi} + |\varepsilon_S|^2)\psi - i\frac{\Gamma}{\omega_\perp}\psi.$$

Here $\tilde{\nabla} = (\partial_\xi, \partial_\eta, \partial_\zeta)$, $\Omega_P = |\mathbf{p}_{12} \cdot \mathbf{e}_x| \mathcal{E}_P / \hbar$ is the half Rabi frequency of the pump field, and $\Phi = \Delta\tilde{k}\zeta - \Delta\tilde{\omega}\tau$ is the phase, with $\Delta\tilde{k} = (k_P \mp k_S)a_\perp$ ("−" for the forward scattering; "+" for the backward scattering) and $\Delta\tilde{\omega} = \Delta_2/\omega_\perp$. Note that since $\omega_\perp \gg \omega_z$, one has $a_\perp \ll a_z$.

Due to the strong transverse confinement provided by the trapping potential, it is possible to factor the solution of Eq. (4) as $\psi = \varphi(\xi, \eta)F(\zeta, \tau)e^{-i\mu\tau}$ [63], with μ the chemical potential and $\varphi(\xi, \eta)$ the transverse mode, governed by the equation

$$-\frac{1}{2}\left(\frac{\partial^2}{\partial\xi^2} + \frac{\partial^2}{\partial\eta^2}\right)\varphi + \frac{1}{2}(\xi^2 + \eta^2)\varphi = \nu\varphi. \tag{5}$$

Note that Eq. (5) has the same form with the eigenvalue equation of a two-dimensional harmonic oscillator in quantum mechanics. When the trapping potential is deep enough, no collective excitations of the Rydberg-dressed BEC can occur in the x and y (transverse) directions, but the occurrence of low-energy excitations induced by the atomic interactions is allowed in the z direction. Furthermore, one can set $\varphi(\xi, \eta) = \varphi_0(\xi, \eta) = e^{-(\xi^2 + \eta^2)/2}$, which is the ground-state solution of Eq. (5) with the eigenvalue $\nu = 1$. In addition, we assume that the scattered field has the same Gaussian transverse distribution with that of φ, with the form $\mathcal{E}_S = g(\zeta, \tau)\mathcal{E}_P e^{-(\xi^2 + \eta^2)/2}$, where $g(\zeta, \tau)$ is a dimensionless function characterizing the amplitude of the scattered field. Since the scattered field is much weaker than the pump one, the magnitude of $g(\zeta, \tau)$ should be much smaller than one.

With the above analysis, Eq. (4) can be simplified into the following (1+1)D form

$$i\frac{\partial F}{\partial\tau} + \frac{1}{2}\frac{\partial^2 F}{\partial\zeta^2} + (\mu - 1)F - \frac{1}{2}\nu^2\zeta^2 F - c_0|F|^2 F$$

$$- c_1 \int d\zeta' U_1(\zeta - \zeta')|F(\zeta', \tau)|^2 F(\zeta, \tau) \tag{6}$$

$$+ c_2\left(1 + \frac{2}{3}ge^{-i\Phi} + \frac{2}{3}g^*e^{i\Phi} + \frac{1}{2}|g|^2\right)F + i\gamma F = 0,$$

where $\nu = \omega_z/\omega_\perp$, $c_0 = 2\pi N a_s/a_\perp$, $c_1 = N/(2\hbar\omega_\perp)$, $c_2 = |\Omega_P|^2/(\omega_\perp\Delta_1)$ and $\gamma = \Gamma/\omega_\perp$. For obtaining Eq. (6), we have multiplied Eq. (4) by $\varphi_0(\xi, \eta)$ and integrated it once with respect to ξ and η.

By using the same approach, Eq. (3) can be converted into the following (1+1)D form

$$i\left(\frac{\partial}{\partial\zeta} + \frac{1}{v}\frac{\partial}{\partial\tau}\right)g + d_0 e^{i\Phi} - d_1 g + d_2\left(\frac{2}{3}e^{i\Phi} + \frac{1}{2}g\right)|F|^2 = 0, \tag{7}$$

with $v = c/(a_\perp\omega_\perp)$, $d_0 = (ca_\perp/\omega_S)(k_P^2 - \omega_P^2/c^2)$, $d_1 = c/(2\omega_S a_\perp)$ and $d_2 = \omega_S|\mathbf{p}_{12} \cdot \mathbf{e}_x|^2 N_0 a_\perp/(2\epsilon_0 c\hbar\Delta_1)$. Equations (6) and (7) are reduced GP-Maxwell equations, both of which are now (1+1)D ones and hence are convenient for an analytical approach.

The model we considered above is rather general. It can be realized by using a Bose-condensed Strontium atomic gas [64] (e.g. ^{88}Sr), with the atomic internal states assigned to be $|1\rangle = |5s^2\ {}^1S_0\rangle$, $|2\rangle = |5s5p\ {}^1P_1\rangle$ and $|3\rangle = |5sns\ {}^1S_0\rangle$. The s-wave scattering length of the BEC is $a_s = 94.8a_0$, with the Bohr radius $a_0 \approx 53$ pm. The spontaneous emission rates of atoms are given by $\Gamma_{12} \approx 2\pi \times 16$ MHz, and $\Gamma_{23} \approx 2\pi \times 16.7$ kHz. The dispersion parameter of the Rydberg state for $n = 60$ is $C_6 \approx 2\pi \times 10.9$ GHz μm^6. Since C_6 is positive, the vdW interaction between atoms in the Rydberg state is attractive, useful to realize a self-focusing Kerr nonlinearity and realize polaritonic solitons. In the following calculations, we assume $\omega_\perp/(2\pi) = 100$ Hz, which results the harmonic oscillator length in the transverse directions $a_\perp \approx 1.1$ μm, $\omega_z/(2\pi) = 0.1$ Hz, which corresponds to the harmonic oscillator length in the longitudinal direction $a_z \approx 32a_\perp \approx 35$ μm, the atomic density $n_0 \approx 2.4 \times 10^{13}$ cm^{-3}, the one-photon (two-photon) detuning $\Delta_1 \approx 50$ MHz ($\Delta_R \approx 18$ GHz), and $\Omega_P \approx \Omega_C \approx 10$ MHz, which gives the Rydberg blockade radius $R_c \approx 4.5$ μm. All calculations given below will be based on these parameters.

3. Linear excitation spectrum and structure factor of the Rydberg-dressed BEC

Now we turn to solve the reduced GP-Maxwell Eqs. (6) and (7). To understand the physical property of the excitations in the system, it is necessary to know the stationary background of the condensate when the scattered laser is absent, which constitutes the base state of the system. Such a based state can be obtained from Eqs. (6) and (7) by neglecting the derivative terms and setting $F = f_0$, $g = 0$, yielding the equations

$$\mu - 1 + c_2 = (c_0 + c_1 u_0)f_0^2, \qquad d_0 + 2d_2 f_0^2/3 = 0, \tag{8}$$

where $u_0 = \int d\zeta' U_1(\zeta - \zeta')$ and we have set $\nu \approx \gamma \approx 0$ as they are small and plays no significant role in the background of the condensate. From the first relation of Eq. (8), one can obtain that $f_0 = \sqrt{(\mu - 1 + c_2)/(c_0 + c_1 u_0)}$. Thus, if the dimensionless length of the BEC is ℓ, corresponding to the length $l = 2a_z\ell$, by using the normalization condition $\int_0^\ell d\zeta f_0^2 = 1$ (derived from $\int d^3r|\Psi|^2 = N$; N is the total number of atoms, which is taken to be 10^3 in the numerical example), the expression of the chemical potential $\mu = 1 - c_2 + (c_0 + c_1 u_0)/\ell$. From the second relation of Eq. (8), we obtain the dispersion relation of the pump laser in the presence of the Rydberg-dressed BEC, i.e. $\omega_P^2/c^2 - k_P^2 = 2\omega_S d_2 f_0^2/(3ca_\perp)$, which can be further reduced to $\omega_P/c = k_P$ when the BEC is absent ($f_0 = 0$).

Now we apply the method of multiple scales [31] to investigate the linear and nonlinear excitations and the propagation behavior of the scattered field in the system. To this end, we make the asymptotic expansions $F = f_0 + \sum_{j=1}^\infty \epsilon^j f^{(j)}$ and $g = \sum_{j=1}^\infty \epsilon^j g^{(j)}$. Here ϵ is a small parameter characterizing the typical amplitude of the scattered field relative to the pump field; all quantities on the right hand side of the expansions are functions of the multi-scale variables $\tau_\alpha = \epsilon^\alpha \tau$ ($\alpha = 0, 1$) and $\zeta_\beta = \epsilon^\beta \zeta$ ($\beta = 0, 1, 2$). The damping parameter γ can be assumed to be the order of ϵ (i.e. $\gamma \sim O(\epsilon)$), which is reasonable because the spontaneous emission is greatly suppressed by the use of the large one-photon detuning Δ_1. With such expansions, Eqs. (6) and (7) are transferred into the form

$$i\left(\frac{\partial}{\partial \tau_0} + \gamma\right)f^{(j)} + \frac{1}{2}\frac{\partial^2 f^{(j)}}{\partial \zeta_0^2} - c_0 f_0^2(f^{(j)} + f^{(j)*}) - c_1 f_0^2 \mathcal{F}[f^{(j)}]$$
$$+ \bar{c}_2 f_0(g^{(j)}e^{-i\phi} + g^{(j)*}e^{i\phi}) = M^{(j)}, \tag{9a}$$

$$i\left(\frac{\partial}{\partial \zeta_0} + \frac{1}{v}\frac{\partial}{\partial \tau_0}\right)g^{(j)} + \bar{d}_2 e^{i\phi} f_0(f^{(j)} + f^{(j)*}) = N^{(j)}, \tag{9b}$$

where $\mathcal{F}[f^{(j)}] = \int d\zeta_0' U(\zeta_0 - \zeta_0')[f^{(j)}(\zeta_0', \zeta_1, \zeta_2, \tau_\alpha) + f^{(j)*}(\zeta_0', \zeta_1, \zeta_2, \tau_\alpha)]$ ($\alpha = 0, 1$), $\phi = \Delta\tilde{k}\zeta_0 - \Delta\tilde{\omega}\tau_0$, $\bar{c}_2 = 2c_2/3$, and $\bar{d}_2 = 2d_2/3$. The explicit expressions for $M^{(j)}$ and $N^{(j)}$ ($j = 1, 2, 3$) at each order are presented in the Supplement 1.

For seeking the density fluctuations of the Rydberg-dressed BEC and the scattered field induced by the pump field, we further assume $f^{(j)} = f_+^{(j)}e^{i\varphi} + f_-^{(j)*}e^{-i\varphi}$, with $\varphi = q\zeta_0 - \omega_q\tau_0$. Here q and ω_q are respectively the dimensionless atomic momentum and the corresponding atomic energy of density fluctuations induced by the light scattering process. Then, Eqs. (9a) and (9b) can be recast into the following equations for $f_+^{(j)}$, $f_-^{(j)}$ and $g^{(j)}$:

$$i\left(\frac{\partial}{\partial \tau_0} + q\frac{\partial}{\partial \zeta_0} + \gamma\right)f_+^{(j)} + \left(\omega_q - \frac{q^2}{2} - c_0 f_0^2\right)f_+^{(j)}$$
$$+ \frac{1}{2}\frac{\partial^2 f_+^{(j)}}{\partial \zeta_0^2} - c_0 f_0^2 f_-^{(j)} - c_1 f_0^2 \tilde{U}(q)f_+^{(j)} + \bar{c}_2 f_0 g^{(j)*}e^{i(\phi-\varphi)} = M^{(j)}e^{-i\varphi}, \tag{10a}$$

$$i\left(\frac{\partial}{\partial\tau_0} - q\frac{\partial}{\partial\zeta_0} + \gamma\right)f_-^{(j)} + \left(\omega_q + \frac{q^2}{2} + c_0f_0^2\right)f_-^{(j)}$$

$$-\frac{1}{2}\frac{\partial^2 f_-^{(j)}}{\partial\zeta_0^2} + c_0f_0^2 f_+^{(j)} + c_1f_0^2\,\tilde{U}(q)f_-^{(j)} - \bar{c}_2 f_0 g^{(j)*}e^{i(\phi-\varphi)} = -M^{(j)*}e^{-i\varphi}, \tag{10b}$$

$$i\left(\frac{\partial}{\partial\zeta_0} + \frac{1}{v}\frac{\partial}{\partial\tau_0}\right)g^{(j)} + \bar{d}_2 f_0(f_+^{(j)*} + f_-^{(j)*})e^{i(\phi-\varphi)} = N^{(j)}, \tag{10c}$$

with the phase difference $\phi - \varphi = (\Delta\tilde{k} - q)\zeta_0 - (\Delta\tilde{\omega} - \omega_q)\tau_0$ and $\tilde{U}(q)$ the Fourier transformation of the nonlocal response function $U(\zeta)$. The phase-matching condition is achieved when $\phi \approx \varphi$, i.e. it is achieved when $q \approx \Delta\tilde{k}$ and $\omega_q \approx \Delta\tilde{\omega}$, simultaneously. Recalling that $\Delta\tilde{k} = (k_P \mp k_S)a_\perp$ ("−" for the forward scattering; "+" for the backward scattering) and $\Delta\tilde{\omega} = \Delta_2/\omega_\perp$, an efficient light scattering will occur only when a linear excitation of the Rydberg-dressed BEC compensates the laser-field phase mismatch. Equations (10a)–(10c) can be solved order by order in a systematic way.

At the first-order ($j = 1$) approximation, under the phase-matching condition ($\phi \approx \varphi$) and assuming that $f_+^{(1)}, f_-^{(1)}$ and $g^{(1)*}$ are all proportional to $e^{i(k\zeta_0 - \omega\tau_0)}$, we obtain the linear dispersion relation

$$(\omega + \omega_q + i\gamma)^2 - (k+q)^2\left[\frac{(k+q)^2}{4} + c_0f_0^2 + c_1f_0^2\tilde{U}(q) + \frac{\bar{c}_2\bar{d}_2 f_0^2}{k - \omega/v}\right] = 0, \tag{11}$$

where $\tilde{U}(q)$ can be found to be $\tilde{U}(q) = Z_0 f(q)$, with $Z_0 = 2\pi\tilde{C}_6/(3R_c^5)$ and

$$f(q) = \frac{1}{2}e^{-|q|R_c/2}\left[e^{-|q|R_c/2} + \cos\left(\frac{\sqrt{3}}{2}|q|R_c\right) + \sqrt{3}\sin\left(\frac{\sqrt{3}}{2}|q|R_c\right)\right]. \tag{12}$$

Particularly, when $|q|R_c \ll 1$, one has $f(q) \approx 1 - q^2R_c^2/4$. Since k is a small deviation from q, we can approximate $k + q \approx q$. As a result, Eq. (11) can be simplified as

$$k(\omega) = \frac{\omega}{v} + \bar{c}_2\bar{d}_2 f_0^2 S(q)\left(\frac{1}{\omega + \omega_q + i\gamma - \omega_B} - \frac{1}{\omega + \omega_q + i\gamma + \omega_B}\right)$$

$$\approx \frac{\omega}{v} + \bar{c}_2\bar{d}_2 f_0^2 S(q)\frac{1}{\omega + \omega_q + i\gamma - \omega_B}, \tag{13}$$

as $1/(\omega + \omega_q + i\gamma + \omega_B) \ll 1/(\omega + \omega_q + i\gamma - \omega_B)$. Here, $S(q) = q^2/(2\omega_B)$, is the structure factor of the Rydberg-dressed BEC, and

$$\omega_B(q) = q\sqrt{q^2/4 + c_0f_0^2 + c_1f_0^2\tilde{U}(q)} = q\sqrt{q^2/4 + c_0f_0^2 + c_1f_0^2 Z_0 f(q)}, \tag{14}$$

is the frequency of the linear (Bogoliubov) excitation in the Rydberg-dressed BEC. Obviously, when the Rydberg dressing is absent ($c_1 = 0$), Eq. (14) is reduced to the standard Bogoliubov spectrum of a normal BEC with only the short-range interaction. Equation (13) presents the linear dispersion relation of a *polariton*, a quasi-particle superposed by the BEC matter-wave and scattered laser field in the system. From Eq. (13), it is obvious that the imaginary part of k is negative around $\omega = 0$, i.e. Im(k)<0 at $\omega \approx 0$. This indicates that the scattered field can acquire an optical gain during the scattering process, which is crucial for the spontaneous generation of the scattered field in the system.

Shown in Fig. 2(a) is the Bogoliubov excitation spectrum of the Rydberg-dressed BEC by taking the oscillating frequency ω_B as a function of qR_c (q is the atomic recoil momentum and R_c is the Rydberg blockade radius). The dashed black line, solid red line, and dotted blue line

in the figure are for the interaction parameter $\alpha \equiv 2n_0c_1f_0^2Z_0 = 10, 80$, and 180, respectively. Particularly, we have $f_0 = 0.32$, $Z_0 = 1.18 \times 10^{-8}$ GHz μm, with the parameters given in the last paragraph of Section 2. Different form conventional BECs with contact interactions, in the Rydberg-dressed BEC the presence of long-range Rydberg-Rydberg interaction can result a significant effect on the the polariton spectrum. Particularly, a maxon maximum followed by a roton minimum can be observed for a moderate value of α, which ultimately results in a roton instability when further increasing α.
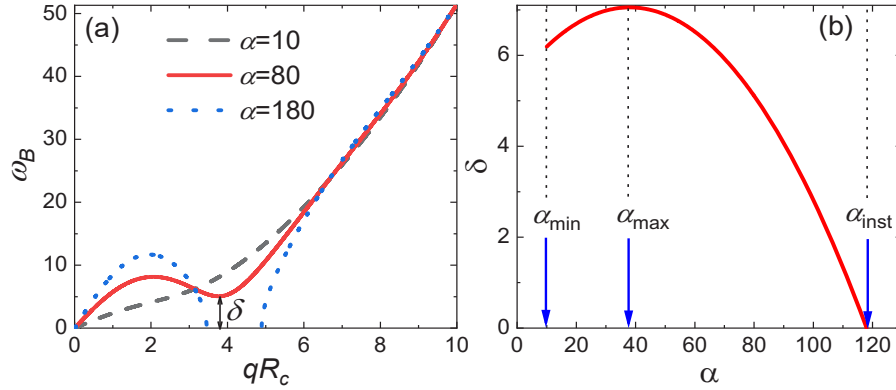
Fig. 2. Linear excitations of the Rydberg-dressed BEC. (a) Linear (Bogoliubov) excitation spectrum ω_B as a function of qR_c (q is the atomic recoil momentum and R_c is the Rydberg blockade radius). The dashed black line, solid red line, and dotted blue line are for the interaction parameter $\alpha = 10, 80$, and 180, respectively; δ denotes the frequency gap for the occurrence of polaritonic roton. (b) Roton gap δ as a function of α. The vertical dashed lines correspond to $\alpha_{\min} \approx 10$, $\alpha_{\max} \approx 38$ and $\alpha_{\text{inst}} \approx 118$, respectively.

The parameter δ in Fig. 2(a) indicates a frequency gap for the local roton minumim, for which ω_B displays the roton minimum at a non-zero value of q. Figure 2(b) shows δ as a function of α. The vertical dashed lines are for $\alpha_{\min} \approx 10$, $\alpha_{\max} \approx 38$ and $\alpha_{\text{inst}} \approx 118$, respectively. We find that δ firstly increases with growth of α until arriving at a critical value $\alpha = \alpha_{\max} \approx 38$; then it decreases as α increases further, and ultimately vanishes at $\alpha = \alpha_{\text{inst}} \approx 118$ which marks the onset of a roton instability.

The structure factor $S(q)$ can significantly affect the dispersive property of the system. Specifically, the system is weakly dispersive when $S(q)$ is small, while it is strongly dispersive when $S(q)$ is large. From the definition of $S(q)$, we have $S(q) \approx q/(2\sqrt{c_0 + c_1Z_0f_0}) \ll 1$ when $q^2/4 \ll c_0f_0^2 + c_1f_0^2\tilde{U}(q)$ and $S(q) \approx 1$ when $q^2/4 \gg c_0f_0^2 + c_1f_0^2\tilde{U}(q)$. Consequently, if the scattered field propagates co-linearly with the pump field (i.e. the forward scattering), one has $q \approx \Delta\tilde{k} \approx (k_P - k_S)a_\perp$, resulting in a small q and hence $S(q) \ll 1$. In such a case, the system is weakly dispersive and has the linear dispersion relation $k \approx \omega/v$. However, if the scattered field propagates anti-co-linearly with the pump field (i.e. the backward scattering), one has $q \approx \Delta\tilde{k} \approx (k_P + k_S)a_\perp$, resulting in a large q and hence $S(q) \approx 1$. In such a scenario, the system is strongly dispersive and has the linear dispersion relation $k \approx \bar{c}_2\bar{d}_2f_0^2/(\omega + \omega_q + i\gamma - \omega_B)$. Since the structure factor of the Rydberg-dressed BEC depends on more system parameters (such as the control-field intensity $|\Omega_c|^2$ and the principal quantum number of Rydberg states n) than that of conventional BECs, the dispersive property of the Rydberg-dressed BEC is more controllable than that of conventional BECs.

Shown in Fig. 3(a) is the structure factor $S(q)$ as a function of the atomic recoil momentum q, for the principle quantum number $n = 30, 60, 90$, and 120, respectively. Note that with the parameters given in the last paragraph of Section 2, we get $\mu \approx -3.64$, $f_0 \approx 0.32$, and $\gamma \approx 0.06$.

We see that $S(q) \approx 0$ when $q \to 0$ and $S(q)$ increases rapidly when q has a small value. However, $S(q) \approx 1$ when $q \to \infty$ and $S(q)$ increases very slowly when q has a large value. Thereby, in the case of forward scattering $q \approx 0$ one has $S(q) \approx 0$ whereas in the case of backward scattering $q \approx 17$ one has $S(q) \approx 1$. Figure 3(b) is an illustration of $S(q)$ as a function of n for different values of q. It is seen that although $S(q)$ always decreases as n increases, it decreases fast (slowly) when q has a small (large) value.
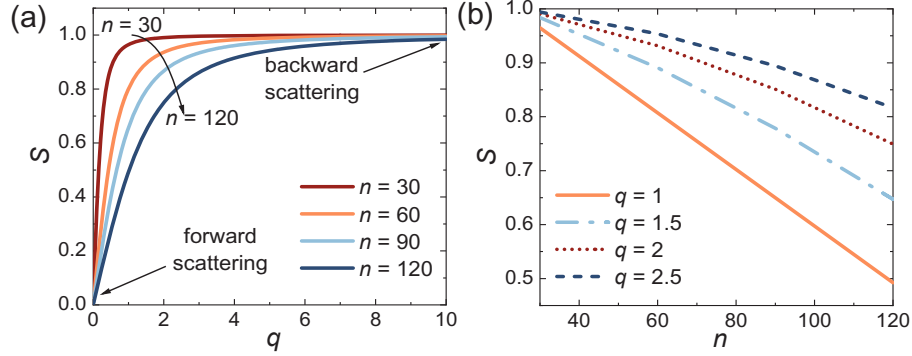
Fig. 3. Structure factor $S(q)$ of the Rydberg-dressed BEC when the roton instability does not occur. (a) $S(q)$ as a function of the atomic recoil momentum q, for the principle quantum number $n = 30$, 60, 90, and 120, respectively. The regions of the forward and backward scattering are indicated. (b) $S(q)$ as a function of n, for $q = 1$ (solid line), 1.5 (dash-dotted line), 2 (dotted line) and 2.5 (dashed line), respectively.

At the first-order approximation, we get solutions $f_+^{(1)} = Ae^{i(k\zeta_0 - \omega\tau_0)}, f_-^{(1)} = aAe^{i(k\zeta_0 - \omega\tau_0)}$, and $g^{(1)*} = bAe^{i(k\zeta_0 - \omega\tau_0)}$, with

$$a = \frac{X}{c_0 f_0^2 + c_1 f_0^2 \tilde{U}(q) + \bar{c}_2 \bar{d}_2 f_0^2 / (k - \omega/v)}, \qquad b = -\frac{\bar{d}_2 f_0}{k - \omega/v}.$$

Here, $X = \omega + \omega_q + i\gamma - q^2/2 - c_0 f_0^2 - c_1 f_0^2 \tilde{U}(q) - \bar{c}_2 \bar{d}_2 f_0^2 / (k - \omega/v)$ and A is a yet to be determined envelope function. The propagation property of the polariton in the linear regime is
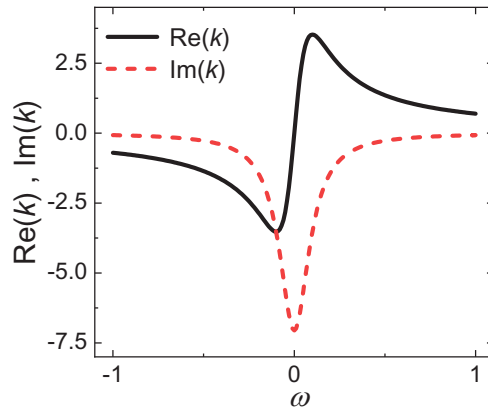
Fig. 4. The linear dispersion relation $k(\omega)$ without occurrence of roton instability as a function of ω. Solid and dashed lines denote the real [Re(k)] and imaginary [Im(k)] parts of $k(\omega)$, respectively.

determined by the linear dispersion relation $k(\omega)$. Particularly, the polariton is stable during the propagation if the imaginary part of $k(\omega)$ [Im(k)] is zero; otherwise, it undergoes an attenuation (amplification) if Im(k) is positive (negative).

Shown in Fig. 4 are real and imaginary parts of $k(\omega)$ [Re(k) and Im(k)] as functions of ω for $\omega_q \approx \omega_B$. It is seen that Re($k$) ≈ 0 and Im(k) arrives at a negative maximum at $\omega \approx 0$, corresponding to a negligible phase shift and a large gain. Thus, the scattered field and hence the polariton can be spontaneously generated and amplified at this point. However, when $|\omega| \gtrsim 1$, one has Re(k) $\gg$ Im(k) ≈ 0, corresponding to a large phase shift and a negligible gain. In these regions, the stable propagation of the scattered field and hence the polariton can be achieved, which will be crucial for the robust propagation of polaritonic solitons.

4. Giant nonlocal Kerr nonlinearity and ultraslow polaritonic solitons

The study of Kerr effect in ultracold atoms is of great interest in nonlinear optics because the Kerr effect is essential for the realization of most nonlinear optical processes and related to many applications [65]. By means of the matter-wave superradiance, it is possible to achieve a significant enhancement of the optical Kerr nonlinearity with controllable nonlocality in the Rydberg-dressed BEC. In order to demonstrate this, we need to go to the high-order solutions of Eq. (10).

At the second order ($j = 2$) approximation, the solvability condition of Eq. (10) requires the condition

$$i\left(\frac{\partial A}{\partial \zeta_1} + \frac{1}{V_g}\frac{\partial A}{\partial \tau_1}\right) = 0, \tag{15}$$

where V_g is the group velocity of the envelope function A, defined by $V_g = [\partial k(\omega)/\partial\omega]^{-1}$. From Eq. (13), we have

$$V_g^{-1} \approx \frac{1}{v} - \bar{c}_2\bar{d}_2f_0^2 S(q)\frac{1}{(\omega_q + i\gamma - \omega_B)^2}\left(1 + \frac{2\omega}{\omega_q + i\gamma - \omega_B}\right). \tag{16}$$

Note that the imaginary part of V_g is much smaller than the corresponding real part under the condition $\gamma \ll \omega_q - \omega_B$ and hence it plays a negligible role.

The evolution of the envelope function A in the nonlinear regime can be obtained by the solvability condition of Eq. (10) at the third-order ($j = 3$) approximation, which yields the nonlinear envelope equation

$$i\frac{\partial A}{\partial \zeta_2} + \frac{D}{2}\frac{\partial^2 A}{\partial \tau_1^2} + \left\{W_1 A \int d\zeta_1' U(\zeta_1 - \zeta_1')|A(\zeta_1', \zeta_2, \tau_1)|^2 \right.$$
$$\left. + W_2 A^* \int d\zeta_1' U(\zeta_1 - \zeta_1')A(\zeta_1', \zeta_2, \tau_1)^2 + W_3|A|^2 A\right\}e^{-2\tilde{\alpha}\zeta_2} = 0, \tag{17}$$

with $D = \partial^2 k(\omega)/\partial\omega^2$, and

$$W_1 = \frac{1}{Z}c_1\alpha_1(|\alpha_1|^2 + 1), \quad W_2 = \frac{1}{Z}c_1\alpha_1,$$

$$W_3 = \frac{1}{Z}\left(2c_0\alpha_1 - \bar{c}_2f_0^2\alpha_1|\beta_1|^2 - \frac{\bar{c}_2\bar{d}_2f_0^2}{k - \omega/v}(1 + |\alpha_1|^2)\beta_1\right).$$

Here, $\alpha_1 = [c_0 + c_1 + \bar{c}_2\bar{d}_2/(k - \omega/v)]f_0^2/[Y - \bar{c}_2\bar{d}_2f_0^2/(k - \omega/v)]$, $\beta_1 = -\bar{d}_2(\alpha_1 + 1)/(k - \omega/v)$, $Y = \omega + \omega_q + i\gamma + q^2/2 + c_1 f_0^2$, $Z = k\alpha_1 - \bar{c}_2 f_0/(k - \omega/v)$, and $\tilde{\alpha} = \epsilon^{-2}\alpha = \epsilon^{-2}$Im($k$). The second term on the left hand side of Eq. (17) related to the coefficient D describes the group-velocity dispersion; the first two terms in the parenthesis (related to coefficients W_1 and W_2) characterize

the nonlocal Kerr nonlinearity, originated from the long-range Rydberg-Rydberg interaction; the last term in the parenthesis (related to the coefficient W_3) characterizes the local Kerr nonlinearity, originated from the short-range contact interaction between the atoms. The coefficients $W_1 \approx 0.7$, $W_2 \approx 0.3$, and $W_3 \approx -0.005$, with the given parameters.

The nonlinear optical effect of the system can be described by the refractive index n, defined by

$$n = n_1 + \int d\zeta' n_2(\zeta - \zeta')|\mathcal{E}_S(\zeta')|^2 + n_3|\mathcal{E}_S|^2, \tag{18}$$

where n_1 denotes the linear refractive index and n_2 (n_3) denotes the nonlocal (local) nonlinear refractive index. They are related to W_1, W_2 and W_3 by the expressions $n_2 = -[c/(\omega_S E_0^2 b^2 a_\perp)](W_1 + W_2)$ and $n_3 = -[c/(\omega_S E_0^2 b^2 a_\perp)]W_3$, respectively. With the given parameters of Strontium atoms and the atomic density $N_0 \approx 2.4 \times 10^{13}$ cm^{-3}, we obtain

$$n_2 \approx 3.63 \times 10^{-7} \text{ m}^2 \text{ V}^{-2}, \ n_3 \approx -1.77 \times 10^{-9} \text{ m}^2 \text{ V}^{-2}. \tag{19}$$

From the above result, it is obvious that n_2 is two orders of magnitude larger than n_3, i.e. the nonlocal Kerr nonlinearity contributed by the Rydberg-Rydberg interaction is much stronger than that of the local one contributed by short-range contact interaction. Moreover, n_2 is about 15 orders of magnitude larger than that obtained in usual nonlinear optical materials, such as optical fibers [66], characterizing a giant nonlocal Kerr nonlinearity.

Now we turn to seek polaritonic soliton solutions based on the nonlinear envelope Eq. (17). To avoid a large gain, one can make ω_q and ω_B slightly different so that the gain peak can be moved away from $\omega = 0$ (see Fig. 4). Compared with the forward scattering, the backward scattering can provide a significant dispersion, which is necessary for balancing the Kerr nonlinearity and hence is crucial for the formation and stable propagation of polaritonic solitons. Combining the Eqs. (15) and (17), we have

$$i\frac{\partial S}{\partial \zeta} + \frac{D}{2}\frac{\partial^2 S}{\partial T^2} + W_1 S \int d\zeta' U(\zeta - \zeta')|S(\zeta', \tau)|^2$$
$$+ W_2 S^* \int d\zeta' U(\zeta - \zeta')S(\zeta', \tau)^2 + W_3|S|^2 S = -i\alpha S, \tag{20}$$

where $S = \epsilon A e^{-\alpha\zeta}$ and $T = \tau - \zeta/V_g$.

Since Eq. (20) is not integrable, we employ a variational method to search possible polaritonic soliton solutions. The Lagrangian of Eq. (20) of the system described by Eq. (20) for $\alpha \approx 0$ is given by $L = \int_{-\infty}^{\infty} \mathcal{L}d\zeta$, where $\mathcal{L}$ is the Lagrangian density, given by $\mathcal{L} = (SS_\zeta^* - S^*S_\zeta) + (D/2)|S_T|^2 - [(W_1 + W_2)/2]|S|^2 \int U(\zeta - \zeta')|S(\zeta', T)|^2 d\zeta' - (W_3/2)|S|^4$. Then, the soliton solutions are sought by the ansatz with a Gaussian wavepacket

$$S = a_s(\zeta) e^{-T^2/[2w_s(\zeta)^2] + ic_s(\zeta)T^2 + i\phi_s(\zeta)}, \tag{21}$$

where a_s denotes the amplitude, w_s is the half peak width, c_s is the wavefront curvature, and ϕ_s is the phase. Substituting the ansatz (21) into the Lagrangian and integrating it over T, one obtains the effective Lagrangian leading further to the equation of a_s by using the Euler-Lagrangian equation. The stationary solution can be acquired by setting $da_s/d\zeta = 0$, which yields the equation

$$\frac{D}{2}\frac{a_s^4}{Q^2} - \frac{\sqrt{2}(W_1 + W_2)}{4}a_s \int d\zeta' U(\zeta - \zeta')a_s(\zeta') - \frac{\sqrt{2}W_3}{4}a_s^2 = 0, \tag{22}$$

where $Q = a_s^2 w_s$ is a propagation constant. By solving Eq. (22) numerically, we get $a_s \approx 0.16$ and $w_s \approx 1.1$, and hence $Q \approx 0.03$. In addition, $c_s = \phi_s = 0$.

We are interested in the stable propagation of the polaritonioc solitons in the system. Returning to the original (i.e., dimensional) variables, the soliton solution for the condensate wave function and the scattered field are respectively given by

$$
\Psi = \frac{N^{1/2}}{a_\perp^{3/2}} \left(f_0 + S e^{i(q+k)z/a_\perp - i(\omega_q + \omega)\omega_\perp t} + a^* S^* e^{-i(q+k)z/a_\perp + i(\omega_q + \omega)\omega_\perp t} \right)
$$
$$
\times e^{-i\mu\omega_\perp t} e^{-(x^2+y^2)/(2a_\perp^2)},
$$
(23)

$$
\mathbf{E}_s = \mathbf{e}_x E_0 b^* S^* e^{-ikz/a_\perp + i\omega\omega_\perp t} e^{-(x^2+y^2)/(2a_\perp^2)}.
$$
(24)

From the solution (23) we see that the collective wave of recoiled atoms consists of two parts, i.e. the left- and right-moving waves along the z axis. With the given system parameters, we have $\mathrm{Re}(a) \approx -1.69 \times 10^{-4}$ and $\mathrm{Re}(b) \approx 0.98$, with their imaginary parts being two orders of magnitude smaller than their corresponding real parts. Since $|a| \ll 1$ and $|b| \sim 1$, almost all recoiled atoms are moving to the right due to the presence of the pump field, while the scattered field is backward propagating. The propagation velocity of the soliton is approximately given by the linear group velocity, estimated to be

$$
V_g = 1.27 \times 10^{-4} \, c,
$$
(25)

which indicates that the propagation of the polaritonic soliton is ultraslow compared with the light speed in vacuum [67].

The input light power of the pump laser for generating the polaritonic soliton can be estimated by computing the Poynting's vector integrated over the cross-sectional area of the condensate, which is given by

$$
P_{\mathrm{gen}} = 2\varepsilon_0 c n_p S_0 \left(\frac{2\hbar}{p_{13}} \right)^2 |\Omega_P|^2 \approx 1.1 \, \mathrm{pW},
$$
(26)

where S_0 is the cross-sectional area ($S_0 \sim 1 \, \mu\mathrm{m}^2$). From the value of P_{gen}, we find that in the present system a very low input power of the pump field is sufficient for generating the polaritonic soliton, which is due to the presence of the giant nonlocal Kerr nonlinearity contributed by the strong Rydberg-Rydberg interaction in the system.

Shown in Fig. 5 is the numerical result of polaritonic soliton, where the soliton amplitude $|E_s/E_0|$ as a function of $T = [\omega_\perp t - z/(a_\perp V_g)]$ and $\zeta = z/a_\perp$ is illustrated. The initial condition used in the simulation is the ansatz (21), with a_s being obtained through solving Eq. (22) numerically. Figure 5(a) shows the case of $(|E_s(\zeta = 0)/E_0|, q) = (1, 4)$. We see that the soliton is robust during propagation. This is because of the exact balance between the dispersion and nonlinearity in the system. Figure 5(b) is for the case $(|E_s(\zeta = 0)/E_0|, q) = (1, 22)$. One sees that the soliton displays significant dispersion, and hence its amplitude (width) decreases (broadens) rapidly during propagation. The reason is that the dispersion (originated by the large atomic recoil momentum q) is much larger than the nonlinearity. The panel (c) of the figure is for $(|E_s(\zeta = 0)/E_0|, q) = (8.5, 1)$. In this situation, the soliton undergoes a collapse due to the fact that the nonlinearity is much larger than the dispersion.

The domains of stable (or unstable) propagation of polaritonic solitons can be obtained by calculating the propagation fidelity, defined by

$$
\mathcal{J} = \frac{|\int_{-\infty}^{\infty} dT S(\zeta = \ell) S(\zeta = 0)|^2}{\int_{-\infty}^{\infty} dT |S(\zeta = \ell)|^2 \int_{-\infty}^{\infty} dT |S(\zeta = 0)|^2}.
$$
(27)

It is obvious that $\mathcal{J} = 1$ at $\zeta = 0$ and $\mathcal{J} \in (0, 1)$ for $0 < \zeta < \ell$. If $\mathcal{J}$ is very close to one in the distance of ℓ, the shape of the soliton can keep nearly invariant during the propagation in this
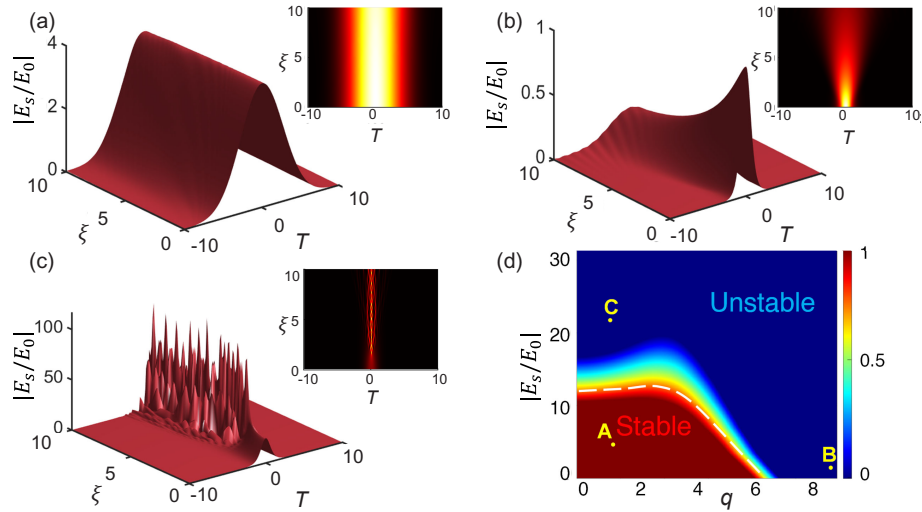
Fig. 5. The formation and propagation of a polaritonic soliton, by taking soliton amplitude $|E_s/E_0|$ as a function of $T = \omega_\perp t - z/(a_\perp V_g)$ and $\zeta = z/a_\perp$. (a) The stable polaritonic soliton solution for the parameters $(|E_s(\zeta = 0)/E_0|, q) = (1, 4)$. Insert: top view of the soliton. (b) The same as (a) but for $(|E_s(\zeta = 0)/E_0|, q) = (1, 22)$. The soliton undergoes significant dispersion during propagation. (c) Also the same as (a) but for $(|E_s(\zeta = 0)/E_0|, q) = (8.5, 1)$. The soliton collapses during propagation. (d) Stability diagram of polaritonic solitons by measuring the propagation fidelity in the parameter plane of the input soliton amplitude $|E_s(\zeta = 0)/E_0|$ and the atomic recoil momentum q. Dots A, B and C represent the cases of panels (a), (b) and (c), respectively. The fidelity shown by the white dashed line is $\mathcal{J} = 0.9$.

distance. However, if $\mathcal{J}$ is close to zero, the shape of the soliton suffers a large distortion during the propagation, i.e. no stable polaritonic solitons are achievable in the system. In Fig. 5(d), we show the stability diagram of polaritonic solitons by measuring the fidelity as a function of the input soliton amplitude $|E_s/E_0|$ and the atomic recoil momentum q. When plotting this figure, polaritonic solitons are assumed to be stable if $\mathcal{J} \gtrsim 0.9$ at $\zeta = \ell = 10$ (corresponding to the length of the BEC ≈ 700 μm), whereas they are unstable if $\mathcal{J} < 0.9$. Dots A, B and C in the figure represent the cases of stable soliton [$\mathcal{J} \approx 1$; corresponding to Fig. 5(a)], dispersive wave [$\mathcal{J} \approx 0$; corresponding to Fig. 5(b)], and collapsed wave [$\mathcal{J} \approx 0$; corresponding to Fig. 5(c)], respectively. We see that polaritonic solitons are stable (unstable) when both $|E_s/E_0|$ and q are small (either $|E_s/E_0|$ or q is large). The boundary between the stable and unstable regions is highlighted by the white dashed line in the figure.

5. Discussion and summary

In this work the Rydberg-dressed BEC is assumed to be described by a single wave function, which is valid only if the recoil energy of the atoms in the BEC is much smaller than that of the atom-photon interaction and that of the atom-atom interaction. In this small recoil-energy regime, excitations of the atoms to high excited states are highly suppressed so that the recoiled atoms mainly remain in the same internal state and the condensate. If the recoil energy is large, the atoms can be scattered from the condensate and generate new side modes. In this case, the description by a single wave function is not applicable. Moreover, the theoretical approach above is built upon a semiclassical description, which is valid only if the numbers of the scattered photons and recoiled atoms are large enough. In addition, to investigate the initial stage of the

superradiance process where scattered photons and recoiled atoms are not large, a fully quantum approach should be used [25–30], which is a topic deserving to be explored in future.

In conclusion, we have presented a scheme for generating nonlocal optical Kerr nonlinearity and polaritonic solitons via matter-wave superradiance in a Rydberg-dressed BEC. We have shown that, due to the strong and long-range interactions between Rydberg atoms, the polariton spectrum of the scattered field is qualitatively different; moreover, the BEC structure factor depends significantly on the Rydberg-dressing and hence is more controllable than that in conventional BECs. We have also shown that such a Rydberg-dressed BEC system supports a giant nonlocal Kerr nonlinearity, and hence allows the formation and stable propagation of polaritonic solitons having ultraslow propagation velocity and ultralow generation power. The results reported here are useful for understanding the unique properties of Rydberg-dressed BECs and have potential applications in optical information processing and transmission.

Disclosures. The authors declare no conflicts of interest.

Data availability. Data underlying the results presented in this paper are not publicly available at this time but may be obtained from the authors upon reasonable request.

Supplemental document. See Supplement 1 for supporting content.

References

1. D. E. Chang, V. Vuletić, and M. D. Lukin, "Quantum nonlinear optics – photon by photon," Nat. Photonics **8**(9), 685–694 (2014).
2. P. D. Drummond and M. Hillery, *The Quantum Theory of Nonlinear Optics*, (Cambridge Univ. Press, Cambridge, UK, 2014).
3. H. Schmidt and A. Imamoğlu, "Giant Kerr nonlinearities obtained by electromagnetically induced transparency," Opt. Lett. **21**(23), 1936 (1996).
4. A. Imamoğlu, H. Schmidt, G. Woods, and M. Deutsch, "Strongly Interacting Photons in a Nonlinear Cavity," Phys. Rev. Lett. **79**(8), 1467–1470 (1997).
5. M. D. Lukin, A. B. Matsko, M. Fleischhauer, and P. Zoller, "Quantum Noise and Correlations in Resonantly Enhanced Wave Mixing Based on Atomic Coherence," Phys. Rev. Lett. **82**(9), 1847–1850 (1999).
6. S. E. Harris and L. V. Hau, "Nonlinear Optics at Low Light Levels," Phys. Rev. Lett. **82**(23), 4611–4614 (1999).
7. M. M. Kash, V. A. Sautenkov, A. S. Zibrov, L. Hollberg, G. R. Welch, M. D. Lukin, Y. Rostovtsev, E. S. Fry, and M. O. Scully, "Ultraslow Group Velocity and Enhanced Nonlinear Optical Effects in a Coherently Dri ven Hot Atomic Gas," Phys. Rev. Lett. **82**(26), 5229–5232 (1999).
8. H. Wang, D. Goorskey, and M. Xiao, "Enhanced Kerr Nonlinearity via Atomic Coherence in a Three-Level Atomic System," Phys. Rev. Lett. **87**(7), 073601 (2001).
9. A. B. Matsko, I. Novikova, G. R. Welch, and M. S. Zubairy, "Enhancement of Kerr nonlinearity by multiphoton coherence," Opt. Lett. **28**(2), 96 (2003).
10. Z.-B. Wang, K.-P. Marzlin, and B. C. Sanders, "Large Cross-Phase Modulation between Slow Copropagating Weak Pulses in ^{87}Rb," Phys. Rev. Lett. **97**(6), 063901 (2006).
11. M. Fleischhauer, A. Imamoglu, and J. P. Marangos, "Electromagnetically induced transparency: Optics in coherent media," Rev. Mod. Phys. **77**(2), 633–673 (2005).
12. M. G. Moore and P. Meystre, "Effects of atomic diffraction on the collective atomic recoil laser," Phys. Rev. A **58**(4), 3248–3258 (1998).
13. D. Kruse, C. von Cube, C. Zimmermann, and Ph. W. Courteille, "Observation of Lasing Mediated by Collective Atomic Recoil," Phys. Rev. Lett. **91**(18), 183601 (2003).
14. M. Vengalattore, M. Hafezi, M. D. Lukin, and M. Prentiss, "Optical Bistability at Low Light Level due to Collective Atomic Recoil," Phys. Rev. Lett. **101**(6), 063901 (2008).
15. S. Inouye, A. P. Chikkatur, D. M. Stamper-Kurn, J. Stenger, D. E. Pritchard, and W. Ketterle, "Superradiant Rayleigh scattering from a Bose-Einstein condensate," Science **285**(5427), 571–574 (1999).
16. S. Inouye, R. F. Low, S. Gupta, T. Pfau, A. Gorlitz, T. L. Gustavson, D. E. Pritchard, and W. Ketterle, "Amplification of light and atoms in a Bose-Einstein condensate," Phys. Rev. Lett. **85**(20), 4225–4228 (2000).
17. D. Schneble, Y. Torii, M. Boyd, E. W. Streed, D. E. Pritchard, and W. Ketterle, "The Onset of Matter-Wave Amplification in a Superradiant Bose-Einstein Condensate," Science **300**(5618), 475–478 (2003).
18. Ö. E. Müstecaplioğlu and L. You, "Superradiant light scattering from trapped Bose-Einstein condensates," Phys. Rev. A **62**(6), 063615 (2000).

19. E. D. Trifonov, "Semiclassical theory of superradiant scattering from a Bose-Einstein condensate," Opt. Spectrosc. **92**(4), 577–583 (2002).

20. H. Pu, W. Zhang, and P. Meystre, "Wave mixing of optical pulses and Bose-Einstein Condensates," Phys. Rev. Lett. **91**(15), 150407 (2003).

21. C. Benedek and M. G. Benedikt, "Cooperative effects in atom field interactions in a Bose-Einstein condensate," J. Opt. B: Quantum Semiclassical Opt. **6**(3), S111–S117 (2004).

22. N. A. Vasilév, O. B. Efimov, E. D. Trifonov, and N. I. Shamrov, "Semiclassical theory of coherent optical effects in Bose-Einstein condensate of dilute atomic gases," Proceedings of the SPIE 5402, 115 (2004).

23. H. Uys and P. Meystre, "Cooperative scattering of light and atoms in ultracold atomic gases," Laser Phys. Lett. **5**(7), 487–502 (2008).

24. Yu. A. Avetisyan and E. D. Trifonov, "Superradiant scattering of light off a dilute Bose-Einstein condensate," Phys. Rev. A **88**(2), 025601 (2013).

25. O. Zobay and G. M. Nikolopoulos, "Dynamics of matter-wave and optical fields in superradiant scattering from Bose-Einstein condensates," Phys. Rev. A **72**(4), 041604 (2005).

26. O. Zobay and G. M. Nikolopoulos, "Spatial effects in superradiant Rayleigh scattering from Bose-Einstein condensates," Phys. Rev. A **73**(1), 013620 (2006).

27. J. Li, X. Zhou, F. Yang, and X. Chen, "Superradiant Rayleigh scattering from a Bose CEinstein condensate with the incident laser along the long axis," Phys. Lett. A **372**(26), 4750–4753 (2008).

28. L. Deng, M. G. Payne, and E. W. Hagley, "Electromagnetic wave dynamics in matter-wave superradiant scattering," Phys. Rev. Lett. **104**(5), 050402 (2010).

29. L. Deng, E. W. Hagley, Q. Cao, X. Wang, X. Luo, R. Wang, M. G. Payne, F. Yang, X. Zhou, X. Chen, and M. Zhan, "Observation of a red-blue detuning asymmetry in matter-wave superradiance," Phys. Rev. Lett. **105**(22), 220404 (2010).

30. L. Deng, C. Zhu, and E. W. Hagley, "Light-wave mixing and scattering with quantum gases," Phys. Rev. Lett. **110**(21), 210401 (2013).

31. C. Hang, G. Gabadadze, and G. Huang, "Giant Kerr nonlinearity and superluminal and subluminal polaritonic solitons in a Bose-Einstein condensate via superradiant scattering," Phys. Rev. A **92**(3), 033805 (2015).

32. P. Meystre, *Atom Optics*, (Springer-Verlag, New York, 2001).

33. A. K. Mohapatra, T. R. Jackson, and C. S. Adams, "Coherent Optical Detection of Highly Excited Rydberg States Using Electromagnetically Induced Transparency," Phys. Rev. Lett. **98**(11), 113003 (2007).

34. T. F. Gallagher, *Rydberg Atoms*, (Cambridge University press, England, 2008).

35. M. Saffman, T. G. Walker, and K. Mølmer, "Quantum information with Rydberg atoms," Rev. Mod. Phys. **82**(3), 2313–2363 (2010).

36. C. S. Adams, J. D. Pritchard, and J. P. Shaffer, "Rydberg atom quantum technologies," J. Phys. B: At., Mol. Opt. Phys. **53**(1), 012002 (2020).

37. S. Sevincli, N. Henkel, C. Ates, and T. Pohl, "Nonlocal Nonlinear Optics in Cold Rydberg Gases," Phys. Rev. Lett. **107**(15), 153001 (2011).

38. C. Murray and T. Pohl, "Quantum and nonlinear optics in strongly interacting atomic ensembles," *Advances in Atomic, Molecular, and Optical Physics* (Academic Press, New York, 2016), Vol. 65, Chap. 7, pp. 321–372.

39. Z. Bai and G. Huang, "Enhanced third-order and Fifth-order Kerr nonlinearities in a cold atomic system via Rydberg-Rydberg interaction," Opt. Express **24**(5), 4442 (2016).

40. Z. Bai, W. Li, and G. Huang, "Stable single light bullets and vortices and their active control in cold Rydberg gases," Optica **6**(3), 309–317 (2019).

41. J. Sinclair, D. Angulo, N. Lupu-Gladstein, K. Bonsma-Fisher, and A. M. Steinberg, "Observation of a Large, Resonant, Cross-Kerr Nonlinearity in a Free-space Rydberg Medium," Phys. Rev. Res. **1**(3), 033193 (2019).

42. A. Tebben, C. Hainaut, V. Walther, Y.-C. Zhang, G. Zürn, T. Pohl, and M. Weidemüller, "Blockade-induced resonant enhancement of the optical nonlinearity in a Rydberg medium," Phys. Rev. A **100**(6), 063812 (2019).

43. Y. Mu, L. Qin, Z. Shi, and G. Huang, "Giant Kerr nonlinearities and magneto-optical rotations in a Rydberg-atom gas via double electromagnetically induced transparency," Phys. Rev. A **103**(4), 043709 (2021).

44. C. Chen, F. Yang, X. Wu, C. Shen, M. K. Tey, and L. You, "Two-color optical nonlinearity in an ultracold Rydberg atom gas mixture," Phys. Rev. A **103**(5), 053303 (2021).

45. N. Henkel, R. Nath, and T. Pohl, "Three-Dimensional Roton Excitations and Supersolid Formation in Rydberg-Excited Bose-Einstein Condensates," Phys. Rev. Lett. **104**(19), 195302 (2010).

46. N. Henkel, F. Cinti, P. Jain, G. Pupillo, and T. Pohl, "Supersolid Vortex Crystals in Rydberg-Dressed Bose-Einstein Condensates," Phys. Rev. Lett. **108**(26), 265301 (2012).

47. J. Honer, H. Weimer, T. Pfau, and H. P. Büchler, "Collective Many-Body Interaction in Rydberg Dressed Atoms," Phys. Rev. Lett. **105**(16), 160404 (2010).

48. F. Maucher, N. Henkel, M. Saffman, W. Królikowski, S. Skupin, and T. Pohl, "Rydberg-Induced Solitons: Three-Dimensional Self-Trapping of Matter Waves," Phys. Rev. Lett. **106**(17), 170401 (2011).

49. C. Gaul, B. J. DeSalvo, J. A. Aman, F. B. Dunning, T. C. Killian, and T. Pohl, "Resonant Rydberg Dressing of Alkaline-Earth Atoms via Electromagnetically Induced Transparency," Phys. Rev. Lett. **116**(24), 243001 (2016).

50. Y. Y. Jau, A. M. Hankin, T. Keating, I. H. Deutsch, and G. W. Biedermann, "Entangling atomic spins with a Rydberg-dressed spin-flip blockade," Nat. Phys. **12**(1), 71–74 (2016).

51. J. Zeiher, R. Van Bijnen, P. Schau, S. Hild, J. Y. Choi, T. Pohl, I. Bloch, and C. Gross, "Many-body interferometry of a Rydberg-dressed spin lattice," Nat. Phys. **12**(12), 1095–1099 (2016).

52. J. Zeiher, J. Y. Choi, A. Rubio-Abadal, T. Pohl, R. van Bijnen, I. Bloch, and C. Gross, "Coherent Many-Body Spin Dynamics in a Long-Range Interacting Ising Chain," Phys. Rev. X **7**, 041063 (2017).

53. E. Guardado-Sanchez, B. M. Spar, P. Schauss, R. Belyansky, J. T. Young, P. Bienias, A. V. Gorshkov, T. Iadecola, and W. S. Bakr, "Quench dynamics of a Fermi gas with strong long-range interactions," Phys. Rev. X **11**, 021036 (2021).

54. J. B. Balewski, A. T. Krupp, A Gaj, S Hofferberth, R Löw, and T Pfau, "Rydberg dressing: understanding of collective many-body effects and implications for experiments," New J. Phys. **16**(6), 063012 (2014).

55. Y. Li, J. Yuan, A. Hemmerich, and X. Li, "Rotation-Symmetry-Enforced Coupling of Spin and Angular Momentum for p-Orbital Bosons," Phys. Rev. Lett. **121**(9), 093401 (2018).

56. V. Borish, O. Markoviiac, J. A. Hines, S. V. Rajagopal, and M. Schleier-Smith, "Transverse-Field Ising Dynamics in a Rydberg-Dressed Atomic Gas," Phys. Rev. Lett. **124**(6), 063601 (2020).

57. M. Viteau, M. G. Bason, J. Radogostowicz, N. Malossi, D. Ciampini, O. Morsch, and E. Arimondo, "Rydberg Excitations in Bose-Einstein Condensates in Quasi-One-Dimensional Potentials and Optical Lattices," Phys. Rev. Lett. **107**(6), 060402 (2011).

58. Z. Zhang, J. Che, D. Zhang, Z. Liu, X. Wang, and Y. Zhang, "Eight-wave mixing process in a Rydberg-dressing atomic ensemble," Opt. Express **23**(11), 13814–13822 (2015).

59. F. Cinti, P. Jain, M. Boninsegni, A. Micheli, P. Zoller, and G. Pupillo, "Supersolid Droplet Crystal in a Dipole-Blockaded Gas," Phys. Rev. Lett. **105**(13), 135301 (2010).

60. G. Pupillo, A. Micheli, M. Boninsegni, I. Lesanovsky, and P. Zoller, "Strongly Correlated Gases of Rydberg-Dressed Atoms: Quantum and Classical Dynamics," Phys. Rev. Lett. **104**(22), 223002 (2010).

61. Y. Li, A. Geissler, W. Hofstetter, and W. Li, "Supersolidity of lattice bosons immersed in strongly correlated Rydberg dressed atoms," Phys. Rev. A **97**(2), 023619 (2018).

62. M. Płodzień, G. Lochead, J. de Hond, N. J. van Druten, and S. Kokkelmans, "Rydberg dressing of a one-dimensional Bose-Einstein condensate," Phys. Rev. A **95**(4), 043606 (2017).

63. V. M. Pérez-García, H. Michinel, and H. Herrero, "Bose-Einstein solitons in highly asymmetric traps," Phys. Rev. A **57**(5), 3837–3842 (1998).

64. S. Stellmer, M. K. Tey, B. Huang, R. Grimm, and F. Schreck, "Bose-Einstein Condensation of Strontium," Phys. Rev. Lett. **103**(20), 200401 (2009).

65. R. W. Boyd, *Nonlinear Optics*, (Academic Press, Amsterdam, 2003).

66. G. P. Agrawal, *Nonlinear Fiber Optics*, 3rd edition (Academic, 2001).

67. P. W. Milonni, *Fast Light, Slow Light and Left-Handed Light*, (Institute of Physics Publishing, 2005).